PCCP

ROYAL SOCIETY OF CHEMISTRY

PAPER

View Article Online
View Journal | View Issue

Cite this: *Phys. Chem. Chem. Phys.*, 2024, **26**, 8195

Differentiating α-moganite, silanol and α-quartz by Raman spectroscopy†

Yasumoto Tsukada, *[ab] Patrick Schmidt [c] and Stephen A. Bowden [a]

Received 2nd November 2023,
Accepted 9th February 2024

DOI: 10.1039/d3cp05330j

rsc.li/pccp

The silica phases quartz, silanol and moganite are widely prevalent and consequential in industrial applications and natural science. However, methods for differentiating these important phases are few. Using Raman spectra simulated by density function and perturbation expansion after discretization theory, representative spectra could be obtained and the comingling of diagnostic Raman Bands for the three phases identified in samples. On this basis new methods to identify moganite in Raman spectra are proposed.

1 Introduction

Quartz is a ubiquitous mineral prevalent on the surface of the Earth and found in all granitic and many sedimentary rocks. Moganite, by comparison, was officially approved as a mineral[1] in 1994 and is difficult to detect thus its occurrence and prevalence are still largely unknown. Based on what is known, it has been suggested that moganite may occur widely and thus it is one of the most under-detected and unrecognised minerals.[2]

Silanol (SiOH) forms where quartz surfaces are exposed to water or inherited within structures as they crystallize (Fig. 1), and thus although silanol has considerable ubiquity, its low effective concentration means that it may largely go unnoticed.[3] This is consequential because both phases have different physico-chemico properties, and thus may alter the way that quartz behaves in many industrial applications (optics, piezo-electric and ceramic materials) as well as in many natural processes (porous media, biomineralization).[4] Thus differentiating and identifying these phases are important.

The purest natural occurrences of moganite are from Gran Canaria Island and were identified by X-ray diffraction.[6,7] But quartz and moganite generate similar diffraction patterns and this makes differentiation of quartz from moganite difficult, this is particularly problematic as the two minerals co-occur and thus the acceptance of moganite as an SiO_2 polymorph

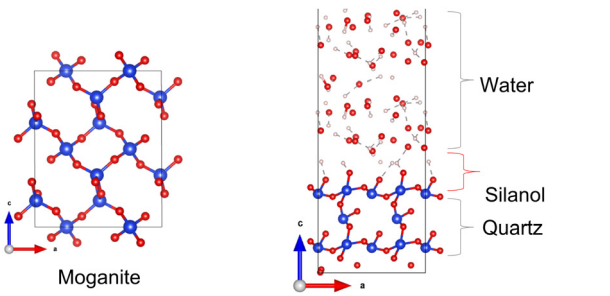

Fig. 1 Structure of moganite and silanol on quartz drawn by VESTA.[5] The blue, red, and white balls represent silicon, oxygen, and hydrogen atoms respectively.

mineralogically distinct from quartz occurred relatively recently.[8] Consequently, Raman spectroscopy came to the fore as a method to distinguish quartz from moganite, a method that has an additional benefit as it is non-destructive.[9] However, while structurally unrelated to moganite, a strong Raman band generated by silanol around 503 cm^{-1}, can mingle with the bands in regions diagnostic for moganite.[10,11] Therefore even if quartz can be distinguished from moganite by its Raman spectra, silanols on the surface, at inner (twinning) surfaces and in the lattice of quartz may still potentially interfere with moganite identification.

As a consequence, reports of the position of Raman bands diagnostic for moganite vary from 500 to 503 cm^{-1}.[9,11–17] Complicating things further is that most peer-reviewed literature concerning moganite does not recognize the potential inference from silanol and the implications it has for moganite analyses. Thus, not only is the extent of the natural occurrence of moganite a polymorph of one the most prevalent minerals unknown,[4] analytical interference in moganite detection remains poorly understood. Here, we present Raman spectroscopic analysis of moganite and silanol on quartz in different sample

[a] *Geosciences, University of Aberdeen, Aberdeen, AB24 3UE, Scotland, UK. E-mail: y.tsukada.21@abdn.ac.uk*
[b] *Japan Organization for Metals and Energy Security, Tokyo, Japan. E-mail: tsukada-yasumoto@jogmec.go.jp*
[c] *Department of Geosciences, Early Prehistory and Quaternary Ecology, Eberhard Karls University of Tübingen, Tübingen, Germany*

† Electronic supplementary information (ESI) available: X-Ray diffraction analysis, Raman spectra and phonon eigendisplacement vector pattern of flint and moganite. See DOI: https://doi.org/10.1039/d3cp05330j

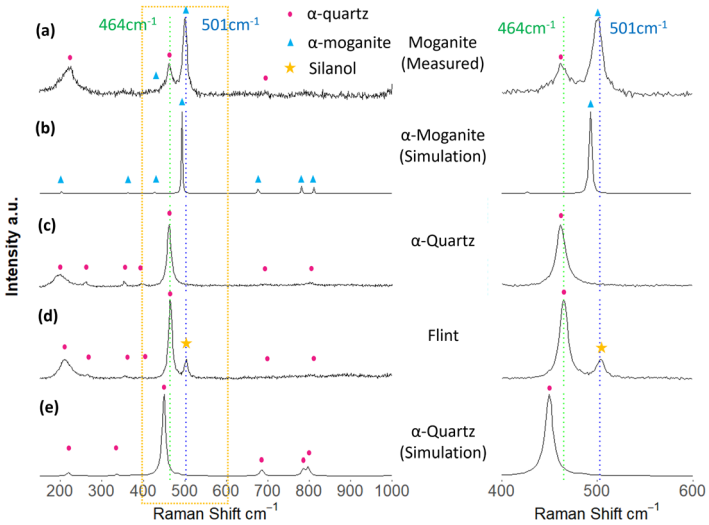

Fig. 2 (a) Measured Raman spectrum of moganite and (b) simulated Raman spectrum of α-moganite, (c) measured spectrum of intact quartz, (d) flint mainly composed of α-quartz associated with a silanol band peak and (e) simulated Raman spectrum of α-quartz. Right hand side; enlarged view of critical region indicated by the yellow box of the left hand side figure. Spectra collected at a laser power of 50% for pristine rocks in Fig. 2(a), (c) and (d).

matrices and demonstrate how Raman spectra simulated by Density Function Theory (DFT)[18,19] and Perturbation Expansion After Discretization (PEAD) confirm moganite phase identifications and measurement.

The major Raman bands reported below 1000 cm^{-1} to be diagnostic for α-moganite (ESI†) are 129, 141, 220, 265, 317, 370 377, 398, 432, 449, 463, 501, 693, 792, and 833 cm^{-1},[9] however, it is still not certain that all these Raman shifts should be assigned to α-moganite, or can be accurately employed for identification purposes (Fig. 2). For example, the band at 220 cm^{-1} is relatively intense compared to others but is of limited use for identifying α-moganite[20,21] (Fig. 2a) because of a lower shifted band at 206 cm^{-1} produced by α-quartz (ESI†) (Fig. 2c).

The rarity of pure reference materials of α-moganite complicates the confirmation of diagnostic Raman bands, and this makes theoretical approaches particularly important thus they have been applied to connect the crystal structure of α-moganite with its vibrational modes in Raman scattering.

Previous work used factor group analysis with the combination of a two-force constant valence potential model to predict optical modes and then conventional lattice dynamic calculations to simulate the vibrational frequencies and the position of bands diagnostic of α- and β-moganite.[22] This approach is helpful but limited to outlining the Raman frequency, but not the relative heights and intensities of bands.

In difference to the previous work, we have used DFT and PEAD simulation (ESI†) under ideal crystallographic data[22] to yield the Raman spectra for α-moganite (Fig. 2b).

2 Experiments

2.1 Samples

In order to avoid confusion about the terminology, the phase and structure names in this document are defined as follows. ''Moganite'', ''Flint'', and ''Quartz'' are used to describe the name of the mineral (powder) sample, while ''α-quartz'', ''α-moganite'' or ''α, β-moganite'' terms the phase name. Silanol is refined as a non-bridged Si–OH band generated on the surface of the minerals (phases), which is not a mineral or phase name itself, to be exact. Two different mineral samples were used for this study. One is a white powder filling taken from Ignimbrite in Gran Canaria, Spain. This sample is used as an end-member phase of α-moganite associated with a minor amount of quartz and halite. The other one is a flint from the museum collection at the University of Aberdeen mainly composed of α-quartz associated with a small amount of silanol band in its Raman spectra (Fig. 2d).

2.2 X-ray diffraction analysis

Reference samples of α-moganite and α-quartz were characterized by powder X-ray diffraction (XRD) prior to Raman analysis (Fig. S1, ESI†). The XRD patterns for samples were acquired using a Panalytical X'Pert powder X-ray diffractometer (Malvern Panalytical) with $CuK_{\alpha1}/K_{\alpha2}$ radiation at the University of Aberdeen. The excitation voltage was 45 kV with a current of 40 mA. Data were collected from 2 to 70° with 0.01 step size and a speed of 85 s per step. The sample of α-moganite is a void-filling mineral deposit and vein that also contains subordinate α-quartz and minor halite. The sample of α-quartz is flint and contains minor impurities (evidenced by peaks around 18, 24, 28, and 31° 2θ CuK_{α}). Also evident from diffractograms in Fig. S1 (ESI†) is the nature of the problem posed by identifying α-moganite by X-ray diffraction; although the lower intensity peaks are visible for moganite and not for quartz, only a small proportion of quartz yields a peak that comingles with peaks diagnostic of α-moganite.

2.3 Raman spectroscopy

The sample of flint was first cut by a diamond saw into pieces small enough to be crushed within a disk mill. Samples of

moganite and flint were then powered within a disk mill to yield powders with a particle size <100 μm. For each sample, powders passing a 38 μm sieve were mixed with distilled water and, based on settling times calculated by Stokes Law, further separated into fractions corresponding to <10, 10–20, 20–30 μm. Fractions were dried in air and mounted on a microscope slide and the surface smoothed with a spatula to minimize roughness.

Raman spectra were measured using a Renishaw in-Via reflex Raman spectrometer housed within a Lecia DMLM reflected light microscope at the University of Aberdeen. Raman spectra were acquired using an Ar^+ green diode laser (514.5 nm) as a monochromatic light source, a 50× objective lens, integration times of 30 000 ms per scan, laser powers of 50 and 100% (as needed see Fig. S3, approximately equating to 0.15 and 0.30 mW, ESI†) and for Raman shifts over the range 100–2000 cm^{-1}. Each acquisition comprised 10 spectra and 10 acquisitions (background-subtracted) were used for each measured spectrum. To improve signal to noise ratios (S/N ratio) synthetic spectra were obtained by normalizing vertical intensities from 0 to 1, summing spectra and dividing by 10. Peak intensities were assigned by taking the highest point, and Full Width at Half Maximum (FWHM) was obtained by fitting curves to individual peaks using Lorentzian broadening within the Fityk[23] software.

3 Computations

3.1 Models and computational simulation

Abinit[18,19] was used for the simulation of density function theory (DFT) calculations. The ideal crystal structure of α-moganite (space group *I*2/*a*) refined in a previous study[22] was used as an input unit cell and the atomic coordinate of the simulation. The exchange and correlation potentials were calculated using Ceperley and Alders Local-density approximation (LDA) with Hartwigsen–Goedeker–Hutter (HGH) pseudopotentials. The Si ($2s^2$, $2p^6$, $3s^2$, $3p^2$) and O ($2s^2$, $2p^4$) valence electrons were treated with a plane wave cutoff of 70 Hartree. To obtain a structural configuration with a high level of convergency for the primitive unit cell, the bulk structures were fully optimized with a cut-off of 100 Hartree cut-off first. The sensitivity test of cut-off energy has confirmed that the total energy of α-moganite has confirmed that the change of the cut-off value from 70 to 100 Hartree results in the change of total energy is 0.12% and the optimized structure has reached the energy close to the ground state. The optimization was set to last until the minimum value of residual cartesian forces was less than $5.0d^{-6}$ Hartree $bohr^{-1}$, as well as the tolerance criteria of the total energy of $1.0d^{-12}$. The Brillouin zone was sampled using a gamma point of the Monkhorst–Pack grid for structural optimization using the Broyden Fletcher Goldfarb Shanno (BFGS) minimization under (2 × 2 × 2) *k*-point mesh for both DFT analysis and following vibrational analysis.

3.2 Vibrational analysis

For vibrational frequency calculation in the harmonic approximation, the force constants were computed by a Perturbation Expansion After Discretization (PEAD) technique implemented in the Abinit package. Following the calculation of the PEAD, the Raman frequency and intensity of the peaks were calculated as follows. The dielectric matrix is calculated for two structures where the atoms are displaced by ±0.01 bohr on each vector of normal mode and derivatives are obtained using a finite difference approach. A postprocessor script, implemented in Abinit, is used to perform the success calculations for Raman operations of normal modes. The intensity calculations were limited to those modes within the frequency range between 100 and 1300 cm^{-1} Raman shifts due to the research focus. To account for spectral line broadening, the intensity of the normal mode was multiplied by a Lorentzian broadening with a 10 cm^{-1} full FWHM.

4 Results and discussion

The phonon eigendisplacement of each Raman-active vibrational frequency (Fig. S5 and S6, ESI†) shows A_g mode at (a) 198 cm^{-1} and (b) 491 cm^{-1}, A_u mode at 220 cm^{-1} and B_g mode at 450 cm^{-1}. A_g, A_u modes are both out-of-plane vibrations that are orthogonal to the *c*-axis while B_g mode is an in-plane movement. This gives an idea of which vibrational property we are measuring through Raman spectroscopy. The highest intensity Raman band in the simulated spectra of α-moganite at 491 cm^{-1} is generated by an A_g mode (Fig. 2b) and corresponds to the Raman band measured at 501 cm^{-1} in the sample of moganite (Fig. 2a). Around 490 cm^{-1} for α-moganite (Fig. 2b) corresponds to a Raman shift of 501 cm^{-1} (Fig. 2a), The second most intense band around 198 cm^{-1} (Fig. 2b and ESI,† Fig. S5) is 1–2 orders of magnitude weaker in intensity compared with the measured data (Fig. 2a). The simulation showed similar low-intensity bands at 670 and 770 cm^{-1} and a very low-intensity band at 430 cm^{-1} (Fig. 2b) that might correspond to the bands measured at 792, 693 and 449 or 463 cm^{-1} (Fig. 2a) while the second most intense band is around 200 cm^{-1} (Fig. 2b), although this peak is 1–2 orders of magnitude weaker in intensity compared with the measured data (Fig. 2a). The simulation showed similar low-intensity bands at 670 and 770 cm^{-1} and a very low-intensity band at 430 cm^{-1} (Fig. 2b) that might correspond to the bands reported for 792, 693 and 449 or 463 cm^{-1},[9] of measured data respectively (Fig. 2a). From a practical perspective using the low-intensity bands to identify α-moganite may not be feasible as the signal-to-noise ratio for many Raman spectra on naturally occurring materials may be too high.

Simulation results represent reasonably well the balance of relative intensity of spectral features, however, uncertainty in the relative intensity remains particularly for bands near 200 cm^{-1} (Fig. 2a), where simulated Raman spectra have a higher intensity than observed in measurements from other studies,[24] but the reversed situation is seen in this study (Fig. 2b). Furthermore, for measurements of moganite some spectral features are likely produced by interference from α-quartz, whereas Raman shifts greater than 501 cm^{-1} should be

assigned to interference with vibrational bands that are normally absent on α-quartz (such as silanol). Therefore, measurements of α-moganite need protocols and sample preparation optimized for the Raman band at 501 cm^{-1}, as other Raman spectra features are too weak or prone to analytical interference. These protocols and preparation methods were evaluated and are presented in the following sections.

To evaluate the effect of surface area and crystal size on the relativity intensities of diagnostic Raman bands, powders of flint and high-purity moganite were measured (silanol and α-quartz for flint and α-moganite and α-quartz for a sample of high purity moganite). For flint, the intensity of the silanol band was much higher in powders with particle sizes <10 μm, with more silanol observed in powders than the intact samples (Fig. 3). This can be explained by crushing and reducing grain size thereby creating fresh surfaces and increasing surface area and hence silanol, and also by exposing silanols originally inherited by internal surfaces or in pore spaces but now physically exposed during sample preparation.[24]

Particle size and crushing had little effect on the relative peak intensities of α-moganite in the sample of high purity moganite, although the moganite powder with a >20 μm particle size evidenced more scatter due to the limited amount of the sample (Fig. 3).

The Raman spectra of flint and moganite also showed a dependence on laser power as well as particle size, especially for flint with particle sizes below 10 μm (Fig. 4). The change to the peak of the α-quartz at 464 cm^{-1} (ESI,† S2 and S3) indicates that the α-quartz was affected by laser-induced heating, as the shift and broadening of the peaks show a similar trend reported in the other studies.[25] The peaks for silanol and α-moganite originating at 503 and 501 cm^{-1} in flint and moganite were both

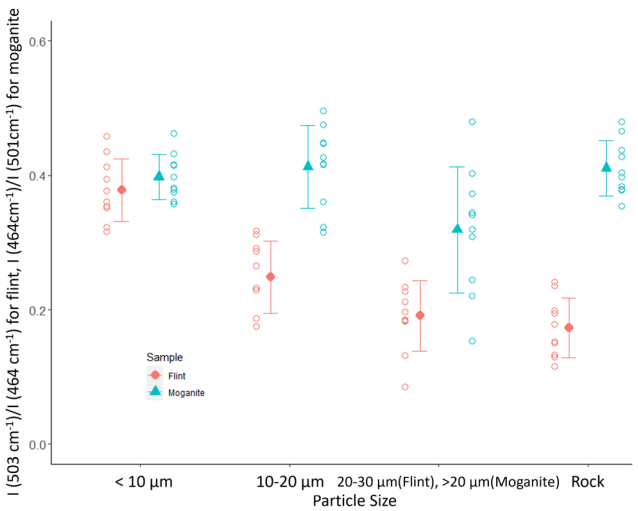

Fig. 3 Silanol/α-quartz and α-quartz/α-moganite for strongest peaks in Raman spectra are shown for flint (red circles) and moganite (blue triangles) depending on their particle size. The closed circles and triangles with the error bars are the average and one standard deviation of the ten measurements. The adjacent open circles are the single points from each acquisition. The exposed incident laser power is 50%.

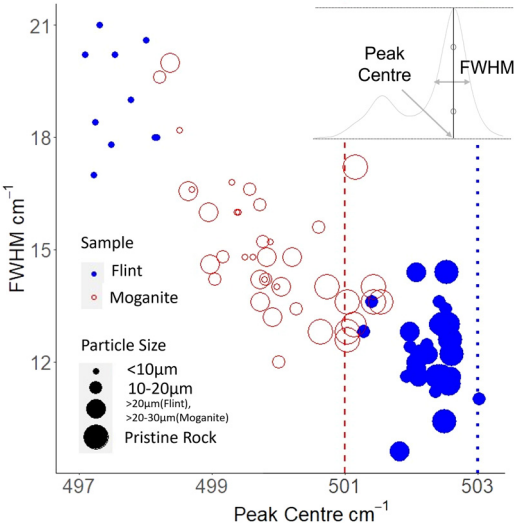

Fig. 4 Changes in Raman spectra at 503 cm^{-1} corresponding to the peak produced by silanol (blue closed circle) and 501 cm^{-1} the peak produced by α-moganite (red open circle). The dashed and dotted vertical lines represent 501 and 503 cm^{-1} respectively. The exposed incident laser power is 100%.

observed to progressively move to lower Raman shifts and exhibited broadening (increase in width) as the laser power was increased. Specifically, the decrease in the Raman shift for the α-moganite peak at 501 cm^{-1}, is interpreted to reflect the rotational movement caused by the phase change of the tetrahedral structure from α- to β-moganite, which was previously observed in X-ray diffraction patterns[22] and supported by Raman spectroscopy measurements made on a heated stage.[12] Similarly, changes for silanol at 503 cm^{-1} caused by the loss of the non-bridging Si–OH silanol band were reported for samples heated up to annealing temperatures (700 °C) from room temperature.[10]

The above changes in Raman spectra can be attributed to phase changes of α-moganite and the loss of the silanol bands, caused by laser-induced heating of surfaces within samples. Despite studies of laser-induced heating in organic materials being common, the effects on non-organic minerals (phases) are not well understood. However, the effects reported in this study are consistent with previous work for α-quartz, which showed that particles with diameters below 11 μm downshifted vibrational frequencies when heated by a high-power laser during Raman spectroscopy.[25] It is also noteworthy that the link movement of peak shifts between silanol and α-quartz suggests the existence of silanol attached to α-quartz (ESI,† S2 and S3).

Measurement of Raman bands at 206 and 220 cm^{-1} showed systematic variation with particle size and laser power indicative of laser-induced heating (Fig. S4, ESI†). This was notably clear for peaks around 206 cm^{-1} measured within the samples of flint (as compared to samples of moganite) where both peak broadening and reduction in Raman shift. This is characteristic of a phase transition from α- to β-quartz.[26] The spectral feature of the peak around 200 cm^{-1} for α-quartz and α-moganite by different particle sizes and laser power were added as Fig. S4

(ESI†). The results showed that both phases are affected by the laser-induced heating, but α-quartz is more vulnerable as well as the silanol band around 503 cm^{-1} of flint. This indicates that the difference in vulnerability is the key feature that can be applied for differentiating two phases.

5 Conclusions

By generating otherwise unavailable pure end-member spectra of α-moganite DFT and PEAD simulations were able to confirm, with the greatest certainty to date, that Raman bands at 501 cm^{-1} are the main diagnostic Raman spectral feature that can be used for α-moganite. This provides much greater confidence than changes in band intensity produced by silanol on α-quartz associated with particle size and laser-induced heating, are distinct from Raman spectra produced by α-moganite. Silanol-bonding on SiO_2-polymorphs, although local in structure, generates strong Raman spectra features and silanol-band intensity increases as particle size decreases and effective surface area increases. Thus, a key finding is that particle size or grain size-related changes in relative band intensity, as well as heating to remove non-bridging silanol, can be used to differentiate moganite and silanol on quartz.

Conflicts of interest

The authors declare that there is no conflict of interest.

Acknowledgements

The authors acknowledge the Japan Organization for Metals and Energy Security for financial support and the use of Maxwell Compute Cluster funded by the University of Aberdeen.

Notes and references

1 L. N. Warr, *Mineral. Mag.*, 2021, **85**, 291–320.
2 P. J. Heaney and J. E. Post, *Science*, 1992, **255**, 441–443.
3 J. Götze, *Mineral. Mag.*, 2009, **73**, 645–671.
4 *Silica: physical behavior, geochemistry and materials applications; [twenty first short course held in conjunction with the annual meetings of the Mineralogical Society of America and the Geological Society of America]*, ed. P. J. Heaney, M. S. of America and G. S. of America, Mineralogical Society of America, Washington, DC, 1994.
5 K. Momma and F. Izumi, *J. Appl. Crystallogr.*, 2011, **44**, 1272–1276.
6 O. W. Flörke, J. B. Jones and H.-U. Schmincke, *Z. Kristallogr. - Cryst. Mater.*, 1976, **143**, 156–165.
7 O. Flörke, U. Flörke and U. Giese, *Neues Jahrb. Mineral., Abh.*, 1984, **149**, 325–336.
8 G. Miehe and H. Graetsch, *Eur. J. Mineral.*, 1992, **4**, 693–706.
9 J. Kingma Kathleen and J. Hemley Russell, *Am. Mineral.*, 1994, **79**, 269–273.
10 P. Schmidt, L. Bellot-Gurlet, A. Slodczyk and F. Fröhlich, *Phys. Chem. Miner.*, 2012, **39**, 455–464.
11 P. Schmidt, L. Bellot-Gurlet, V. Leá and P. Sciau, *Eur. J. Mineral.*, 2014, **25**, 797–805.
12 P. J. Heaney, D. A. McKeown and J. E. Post, *Am. Mineral.*, 2007, **92**, 631–639.
13 A. M. Alonso-Zarza, M. Ángeles Bustillo, J. L. Pérez-Jiménez and M. Furio, *Spectrosc. Lett.*, 2012, **45**, 109–113.
14 J. Götze, L. Nasdala, R. Kleeberg and M. Wenzel, *Contrib. Mineral. Petrol.*, 1998, **133**, 96–105.
15 J. Götze, K. Stanek, G. Orozco, M. Liesegang and T. Mohr-Westheide, *Minerals*, 2021, **11**, 531.
16 M. Sitarz, P. Wyszomirski, B. Handke and P. Jeleń, *Spectrochim. Acta, Part A*, 2014, **122**, 55–58.
17 D. Pop, C. Constantina, D. Tatar and W. Kiefer, *Raman spectroscopy on gem-quality microcrystalline and amorphous silica varieties from Romania*, Studia Universitatis Babes-Bolyai, Geologia, 2004, vol. 49, pp. 41–52.
18 X. Gonze, B. Amadon, G. Antonius, F. Arnardi, L. Baguet, J.-M. Beuken, J. Bieder, F. Bottin, J. Bouchet, E. Bousquet, N. Brouwer, F. Bruneval, G. Brunin, T. Cavignac, J.-B. Charraud, W. Chen, M. Côté, S. Cottenier, J. Denier, G. Geneste, P. Ghosez, M. Giantomassi, Y. Gillet, O. Gingras, D. R. Hamann, G. Hautier, X. He, N. Helbig, N. Holzwarth, Y. Jia, F. Jollet, W. Lafargue-Dit-Hauret, K. Lejaeghere, M. A. L. Marques, A. Martin, C. Martins, H. P. C. Miranda, F. Naccarato, K. Persson, G. Petretto, V. Planes, Y. Pouillon, S. Prokhorenko, F. Ricci, G.-M. Rignanese, A. H. Romero, M. M. Schmitt, M. Torrent, M. J. van Setten, B. V. Troeye, M. J. Verstraete, G. Zérah and J. W. Zwanziger, *Comput. Phys. Commun.*, 2020, **248**, 107042.
19 A. H. Romero, D. C. Allan, B. Amadon, G. Antonius, T. Applencourt, L. Baguet, J. Bieder, F. Bottin, J. Bouchet, E. Bousquet, F. Bruneval, G. Brunin, D. Caliste, M. Côté, J. Denier, C. Dreyer, P. Ghosez, M. Giantomassi, Y. Gillet, O. Gingras, D. R. Hamann, G. Hautier, F. Jollet, G. Jomard, A. Martin, H. P. C. Miranda, F. Naccarato, G. Petretto, N. A. Pike, V. Planes, S. Prokhorenko, T. Rangel, F. Ricci, G.-M. Rignanese, M. Royo, M. Stengel, M. Torrent, M. J. van Setten, B. V. Troeye, M. J. Verstraete, J. Wiktor, J. W. Zwanziger and X. Gonze, *J. Chem. Phys.*, 2020, **152**, 124102.
20 K. A. Rodgers and W. A. Hampton, *Mineral. Mag.*, 2003, **67**, 1–13.
21 K. A. Rodgers and G. Cressey, *Mineral. Mag.*, 2001, **65**, 157–167.
22 P. J. Heaney and J. E. Post, *Am. Mineral.*, 2001, **86**, 1358–1366.
23 M. Wojdyr, *J. Appl. Crystallogr.*, 2010, **43**, 1126–1128.
24 D. Pankin, M. Smirnov, E. Roginskii, A. Savin, I. Kolesnikov and A. Povolotckaia, *Photonics*, 2023, **10**, 1346.
25 C. H. Chio, S. K. Sharma, P. G. Lucey and D. W. Muenow, *Appl. Spectrosc.*, 2003, **57**, 774–783.
26 C. V. Raman and T. M. K. Nedungadi, *Nature*, 1940, **145**, 147.